J Solid State Electrochem (2012) 16:491–497
DOI 10.1007/s10008-011-1357-0

ORIGINAL PAPER

Electrochemical behavior of spherical $LiNi_{1/3}Co_{1/3}Mn_{1/3}O_2$ as cathode material for aqueous rechargeable lithium batteries

Li Liu · Fanghua Tian · Xingyan Wang · Zhenhua Yang · Quanqi Chen · Xianyou Wang

Received: 13 December 2010 / Revised: 24 February 2011 / Accepted: 28 February 2011 / Published online: 6 April 2011

Abstract Spherical $LiNi_{1/3}Co_{1/3}Mn_{1/3}O_2$ powders have been synthesized from co-precipitated spherical metal hydroxide. The electrochemical performances of the $LiNi_{1/3}Co_{1/3}Mn_{1/3}O_2$ electrodes in 1 M $LiNO_3$, 5 M $LiNO_3$, and saturated $LiNO_3$ aqueous electrolytes have been studied using cyclic voltammetry and ac impedance tests in this work. The results show that $LiNi_{1/3}Co_{1/3}Mn_{1/3}O_2$ electrode in saturated $LiNO_3$ electrolyte exhibits the best electrochemical performance. An aqueous rechargeable lithium battery containing $LiNi_{1/3}Co_{1/3}Mn_{1/3}O_2$ cathode, $LiV_{2.9}Ni_{0.050}Mn_{0.050}O_8$ anode, and saturated $LiNO_3$ electrolyte is fabricated. The battery delivers an initial capacity of 98.2 mAh g^{-1} and keeps a capacity of 63.9 mAh g^{-1} after 50 cycles at a rate of 0.5 C (278 mA g^{-1} was assumed to be 1 C rate).

Keywords Aqueous electrolyte · Electrochemical performance · $LiNi_{1/3}Co_{1/3}Mn_{1/3}O_2$ · Aqueous rechargeable lithium batteries (ARLBs)

L. Liu · F. Tian · X. Wang · Z. Yang · Q. Chen · X. Wang (✉)
School of Chemistry, Key Laboratory of Environmentally Friendly Chemistry and Applications of Ministry of Education, Key Laboratory of Materials Design and Preparation Technology of Hunan Province, Xiangtan University,
Xiangtan 411105, China
e-mail: xywang@xtu.edu.cn

L. Liu (✉) · Z. Yang
Faculty of Materials, Optoelectronics and Physics, Xiangtan University,
Xiangtan 411105, China
e-mail: liuli@xtu.edu.cn

Introduction

Rechargeable lithium ion batteries with nonaqueous electrolytes have been widely commercially used due to their high energy density and high working potential. Although nonaqueous organic electrolytes have wide electrochemical window, they have the drawbacks of flammability, low conductivity, and high cost. Usually, they contain flammable organic electrolytes which might cause the production of intense smoke or even fire in the case of improper use such as overcharging or short-circuiting [1, 2]. Furthermore, organic lithium ion batteries are comparatively expensive due to special cell design, necessity of a perfect dry environment during manufacturing processes, and costly organic electrolytes [1, 2].

In the mid-1990s, aqueous rechargeable lithium battery (ARLB) that uses 5 M $LiNO_3$ aqueous electrolyte and incorporates VO_2 as the anode and $LiMn_2O_4$ as the cathode was proposed by Dahn et al. and attracted a lot of attention [3, 4]. Aqueous electrolytes have the advantages of good safety performance and low cost. By this combination, the safety problem of the organic electrolyte is fundamentally resolved, the ion conductivity of the electrolyte is enhanced by several magnitudes, and the rigorous assembly conditions are avoided so the cost is reduced greatly, compared with the nonaqueous lithium ion battery[5].

After searching for a long time, researchers have found that many Li-ion intercalated compounds, such as $LiNi_{0.81}Co_{0.19}O_2$ [6], $LiCoO_2$ [7, 8], $LiMn_2O_4$ [5, 9], and $LiNi_{1/3}Co_{1/3}Mn_{1/3}O_2$ [10, 11] can be used as cathode materials for ARLBs. The anode material researches for ARLBs focus on vanadium oxides, especially for LiV_3O_8 because of its higher capacity than other materials [6, 7, 9]. Various

aqueous electrolytes have been used in ARLBs, such as 1 M $LiNO_3$ [12], 5 M $LiNO_3$ [3, 13, 14], saturated (~9 M) $LiNO_3$ [7, 15, 16], 0.5 M Li_2SO_4 [17], 1 M Li_2SO_4 [10, 18], 2 M Li_2SO_4 [9], saturated Li_2SO_4 [1], LiOH [19], and 1 M LiCl [6]. During the electrolytes mentioned above, $LiNO_3$ solutions are the most commonly used electrolytes. It is evident that the matching ability of aqueous electrolytes and electrode materials is very important for ARLBs. The electrochemical behaviors of $LiCoO_2$ in 0.5 M and saturated aqueous Li_2SO_4 solutions have been studied by Y. P. Wu and coworkers [17, 20]. Ruffo et al. [8] studied the electrochemical performance of $LiCoO_2$ in different $LiNO_3$ electrolytes (0.1 M, 1 M, and 5 M) and found that $LiCoO_2$ in 5 M $LiNO_3$ electrolyte exhibited the best electrochemical performance. Tian et al. [21] studied the electrochemical performance of $LiMn_2O_4$ in different aqueous electrolytes and found that $LiMn_2O_4$ in 5 M $LiNO_3$ electrolyte exhibits good electrochemical performance.

As we know, $LiNi_{1/3}Co_{1/3}Mn_{1/3}O_2$ is one of the most promising alternative materials for $LiCoO_2$ due to its lower price and better safety performance than $LiCoO_2$ [22]. And due to stable cycling performances, safety, and rate capability of $LiNi_{1/3}Co_{1/3}Mn_{1/3}O_2$, this material is considered to be one of the best candidates of positive electrode material for hybrid electric vehicle power source system [22, 23]. A large number of studies on the electrochemical behavior of $LiNi_{1/3}Co_{1/3}Mn_{1/3}O_2$ as a positive electrode material in nonaqueous lithium ion batteries have been reported [24, 25]. Furthermore, spherical $LiNi_{1/3}Co_{1/3}Mn_{1/3}O_2$ shows high tap density and attracts a lot of attention [26, 27]. Despite the large number of studies on the electrochemical behavior of $LiNi_{1/3}Co_{1/3}Mn_{1/3}O_2$ as a positive electrode material in nonaqueous lithium ion batteries, little information is available about the electrochemical behavior of $LiNi_{1/3}Co_{1/3}Mn_{1/3}O_2$ as a positive electrode material in aqueous rechargeable lithium batteries (ARLBs).The electrochemical behavior of $LiNi_{1/3}Co_{1/3}Mn_{1/3}O_2$ in 1 M Li_2SO_4 solution electrolyte has been studied [10], and LiV_3O_8// $LiNi_{1/3}Co_{1/3}Mn_{1/3}O_2$ ARLB system with Li_2SO_4 solution electrolyte has been proposed by Wang et al. [11]. Zheng et al. [28] studied the electrochemical performance of $LiNi_{1/3}Co_{1/3}Mn_{1/3}O_2$ in 2 M $LiNO_3$ electrolyte and found that $LiNi_{1/3}Co_{1/3}Mn_{1/3}O_2$ had excellent electrochemical performances in $LiNO_3$ aqueous solution. However, the electrochemical behavior of LiV_3O_8//$LiNi_{1/3}Co_{1/3}Mn_{1/3}O_2$ ARLB system with $LiNO_3$ solution electrolyte has not been studied.

In this work, we synthesized spherical $LiNi_{1/3}Co_{1/3}Mn_{1/3}O_2$ by a classic co-precipitated method and investigated the electrochemical behavior of $LiNi_{1/3}Co_{1/3}Mn_{1/3}O_2$ in aqueous $LiNO_3$ solutions at different concentrations. And an ARLB system with saturated $LiNO_3$ electrolyte, $LiNi_{1/3}Co_{1/3}Mn_{1/3}O_2$ cathode, and Ni, Mn co-doped LiV_3O_8 ($LiV_{2.9}Ni_{0.050}Mn_{0.050}O_8$) anode has been proposed. $LiV_{2.9}Ni_{0.050}Mn_{0.050}O_8$ has been reported by our pervious paper and shows much better electrochemical performances than pristine LiV_3O_8 [29].

Experimental

Preparation of material

Spherical $LiNi_{1/3}Co_{1/3}Mn_{1/3}O_2$ powders were synthesized from spherical $(Ni_{1/3}Co_{1/3}Mn_{1/3})(OH)_2$ by a classic co-precipitation method [22].

$LiV_{2.9}Ni_{0.050}Mn_{0.050}O_8$ was synthesized by our previously reported method [29]. Briefly, $LiV_{2.9}Ni_{0.050}Mn_{0.050}O_8$ was synthesized by a peroxide sol–gel method from stoichiometric amounts of V_2O_5, $LiOH{\cdot}H_2O$, $Ni(CH_3COO)_2{\cdot}4H_2O$, and $Mn(CH_3COO)_2{\cdot}4H_2O$. Detailed procedure can be seen in our previous paper [29].

Material characterizations

The synthesized $LiNi_{1/3}Co_{1/3}Mn_{1/3}O_2$ was characterized by X-ray powder diffraction (XRD) using a Rigaku D/MAX-3C powder diffractometer with a graphite monochromatic and Cu Kα radiation (λ=0.15418 nm) in the 2θ range of 10–80°. Scanning electron microscope image of the sample was observed using a JEOL JSM-6610 scanning election microscope.

Electrochemical measurements

The electrode was prepared by pressing a powdered mixture of the active material ($LiNi_{1/3}Co_{1/3}Mn_{1/3}O_2$ or $LiV_{2.9}Ni_{0.050}Mn_{0.050}O_8$), acetylene black and polyvinylidene fluoride in a weight ratio of 85:10:5 onto a stainless steel mesh at 10 Mpa.

A three-electrode electrochemical cell was employed for the measurement of cyclic voltammograms (CV) in 1 M $LiNO_3$, 5 M $LiNO_3$, and saturated $LiNO_3$ aqueous electrolytes. The pH value of 1 M, 5 M, and saturated $LiNO_3$ aqueous solutions are 6.105, 5.75, and 4.903, respectively (characterized by a Shanghai Rex PHS-3C pH meter). The prepared $LiNi_{1/3}Co_{1/3}Mn_{1/3}O_2$ electrode, a saturated calomel electrode (SCE), and a stainless steel mesh were used as work, reference, and counter electrode, respectively. Cyclic voltammetry (CV) tests were performed on a Zahner Zennium electrochemical workstation at various scan rates (1, 2, 5, or 10 mv s^{-1}).

A CR2025-type coin cell was employed for the measurement of electrochemical impedance spectroscopy

(EIS) and galvanostatic charge–discharge tests. The testing cells were assembled with the $LiNi_{1/3}Co_{1/3}Mn_{1/3}O_2$ cathode thus fabricated, $LiV_{2.9}Ni_{0.050}Mn_{0.050}O_8$ anode, sulfonated polyolefin separator (provided by Hunan Corun New Energy Co., Ltd., China), and electrolyte (1 M, 5 M, or saturated $LiNO_3$ aqueous electrolytes). The mass loading of the cathode and anode depends on the capacity balancing ratio of cathode to anode. EIS experiments were carried out before cycle by using a Zahner Zennium electrochemical workstation. The ac perturbation signal was ±5 mV, and the frequency range was from 10 mHz to 10^5 Hz. Galvanostatic discharge and charge tests were run at various current rates between 0.5 and 1.5 V. The cell capacity was determined by the weight of $LiNi_{1/3}Co_{1/3}Mn_{1/3}O_2$.

Results and discussion

Characterization of $LiNi_{1/3}Co_{1/3}Mn_{1/3}O_2$

The XRD patterns of the $Li[Ni_{1/3}Co_{1/3}Mn_{1/3}]O_2$ are shown in Fig. 1.The sample has typical hexagonal α-$NaFeO_2$ structure (space group: 166, $R-\overline{3}m$), no secondary phase is observed in the figure. The narrow diffraction peaks indicate the high crystalline of both $Li[Ni_{1/3}Co_{1/3}Mn_{1/3}]O_2$ powders. Clear peak splits of (006)/(102) and (018)/(110) can be observed in Fig. 1, which indicate the formation of highly ordered layered structure for both $Li[Ni_{1/3}Co_{1/3}Mn_{1/3}]O_2$ powders [30].

Figure 2 shows the scanning electron micrographs of the final product $Li[Ni_{1/3}Co_{1/3}\ Mn_{1/3}]O_2$. It can be seen from Fig. 2a that prepared $Li[Ni_{1/3}Co_{1/3}\ Mn_{1/3}]O_2$ powders show spherical particles with diameter of 5–10 μm. As shown in Fig. 2b, each of spherical particles is made up of a large number of primary grains with less than 1 μm in diameter. Usually, this kind of spherical morphology could favor to enhance high rate capability of the material [31]. Generally, the intercalation process of Li^+ between the layers of $Li[Ni_{1/3}Co_{1/3}\ Mn_{1/3}]O_2$ is a diffusion process, so small grains (high surface area) are beneficial to intercalation, and good electrochemical performance of $Li[Ni_{1/3}Co_{1/3}\ Mn_{1/3}]O_2$ can be expected, but tapping density is small. However, as can be seen in Fig. 2, the primary particle size is less than 1 μm in diameter and these small particles aggregated with each other to form spherical secondary particle. Thus, this kind of morphology could be thought to enhance high rate capability with respect to high surface area without decreasing tapping density.

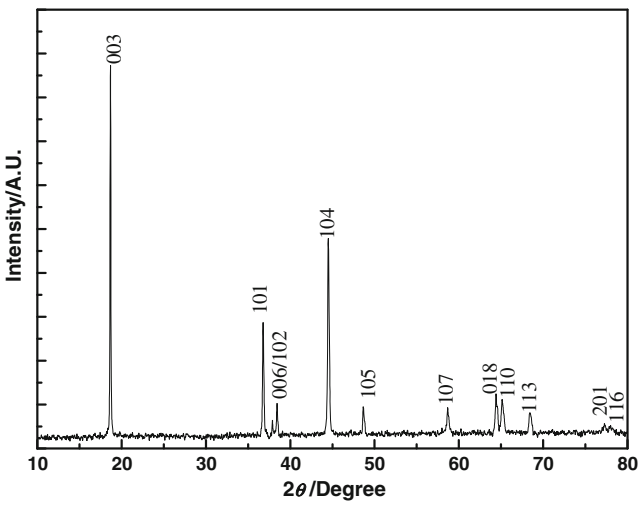

Fig. 1 XRD pattern of $LiNi_{1/3}Co_{1/3}Mn_{1/3}O_2$

Electrochemical studies of $LiNi_{1/3}Co_{1/3}Mn_{1/3}O_2$ in different aqueous electrolytes

The comparison of the second cyclic voltammograms $LiNi_{1/3}Co_{1/3}Mn_{1/3}O_2$ electrode in different aqueous $LiNO_3$ solutions at a scan rate of 1 mV s^{-1} is shown in Fig. 3. It is known that the areas surrounded by CVs are proportional to special capacities [32]. The area under the peak by CV of $LiNi_{1/3}Co_{1/3}Mn_{1/3}O_2$ electrode in saturated $LiNO_3$ solution is the largest as shown in Fig. 3, so the largest specific capacity of $LiNi_{1/3}Co_{1/3}Mn_{1/3}O_2$ electrode in saturated $LiNO_3$ solution could be expected. All cyclic voltammograms show a pair of obvious redox peaks. The anodic peak is ascribed to lithium insertion process for $LiNi_{1/3}Co_{1/3}Mn_{1/3}O_2$, and the cathodic peak is ascribed to lithium deintercalation process for $LiNi_{1/3}Co_{1/3}Mn_{1/3}O_2$. The electrochemical mechanisms will be discussed later. The redox peaks of $LiNi_{1/3}Co_{1/3}Mn_{1/3}O_2$ electrode in1 M $LiNO_3$ solution are located at 0.718 and 0.362 V. At the higher concentrations, the current peaks were quite sharp, and the positions of the cathodic and anodic peak potentials were quite close. The redox peaks of $LiNi_{1/3}Co_{1/3}Mn_{1/3}O_2$ electrode in 5 M $LiNO_3$ solution were located at 0.874 and 0.518 V. The redox peaks of $LiNi_{1/3}Co_{1/3}Mn_{1/3}O_2$ electrode in saturated $LiNO_3$ solution were located at 0.815 and 0.565 V. The position difference between cathodic and anodic peak is the smallest. This indicates fast kinetics. The above results suggest that the reversibility and reactivity of $LiNi_{1/3}Co_{1/3}Mn_{1/3}O_2$ electrode in saturated $LiNO_3$ solution are better than that in 5 M $LiNO_3$ and 1 M $LiNO_3$, and the electrochemical performances of $LiNi_{1/3}Co_{1/3}Mn_{1/3}O_2$ electrode in saturated or 5 M $LiNO_3$ solution that are much superior to that in 1 M $LiNO_3$ solution are demonstrated.

The Nyquist plots of $LiV_{2.9}Ni_{0.050}Mn_{0.050}O_8$//$LiNi_{1/3}Co_{1/3}Mn_{1/3}O_2$ ARLB in different electrolytes are shown in Fig. 4. As can be seen, each of the Nyquist plots consists of an arc and a line. The intercept at the Z_{real} (Z') axis in the

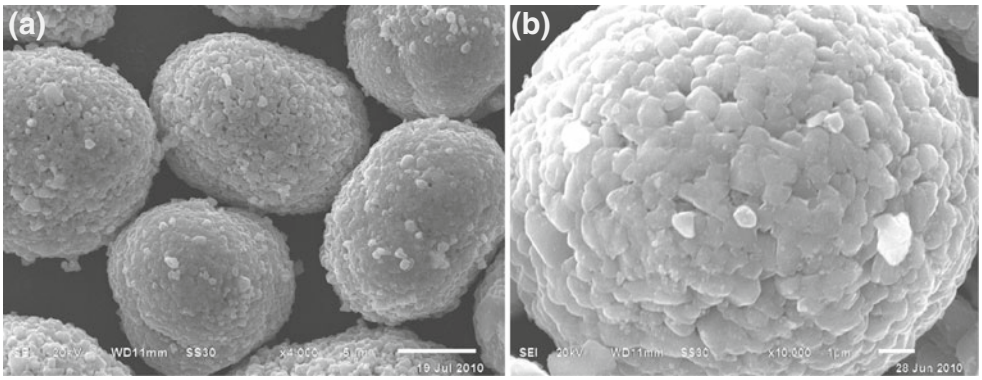

Fig. 2 Scanning electron micrograph of as-prepared $LiNi_{1/3}Co_{1/3}Mn_{1/3}O_2$ particles with different magnifications, the magnification in **a** is ×4,000, and the magnification in **b** is ×10,000

high frequency refers to R_s, which includes electrolyte solution resistance and electric contacts resistance. The semi-circle in the high and middle frequency range is due to the charge transfer resistance (R_{ct}), and the sloping line in the lower frequency represents lithium-ion diffusion resistance in electrode bulk, namely the Warburg impedance. The Nyquist plots were fitted using the equivalent circuit model (inset in Fig. 4), and the fitted impedance parameters are listed in Table 1. The equivalent circuit model includes electrolyte resistance R_s, a constant phase element associated with the interfacial resistance, charge transfer resistance R_{ct}, and the Warburg impedance (Z_w) that is related to the diffusion of lithium ions in the solid oxide matrix. The R_s and R_{ct} of cell in saturated $LiNO_3$ solution are 2.586 and 59.78 Ω respectively, which are increased a little in 5 M $LiNO_3$ solution, while the R_s and R_{ct} are increased remarkably in 1 M $LiNO_3$ solution, especially for R_{ct}. According to Chen et al.'s [33] studies on EIS of lithium-ion cells, the cell impedance is mainly attributed to the charge transfer resistance. Therefore, it can be assumed that $LiV_{2.9}Ni_{0.050}Mn_{0.050}O_8$//$LiNi_{1/3}Co_{1/3}Mn_{1/3}O_2$ ARLB in saturated $LiNO_3$ solution would show better electrochemical properties than in 1 M and 5 M $LiNO_3$ solutions.

Electrochemical studies of $LiV_{2.9}Ni_{0.050}Mn_{0.050}O_8$//$LiNi_{1/3}Co_{1/3}Mn_{1/3}O_2$ ARLB with saturated $LiNO_3$ solution electrolyte

The cyclic voltammograms of the prepared $LiNi_{1/3}Co_{1/3}Mn_{1/3}O_2$ and $LiV_{2.9}Ni_{0.050}Mn_{0.050}O_8$ electrodes in the saturated $LiNO_3$ solution electrolyte at a scan rate of 1 mV/s are shown in Fig. 5. It can be seen that the hydrogen and oxygen evolutions occurs at about −1.2 and 1.8 V vs. saturated calomel electrode (SCE), respectively, due to overpotentials. In the case of $LiV_{2.9}Ni_{0.050}Mn_{0.050}O_8$, one pair of redox peaks located at −0.346 (red. 1) and −0.142 V

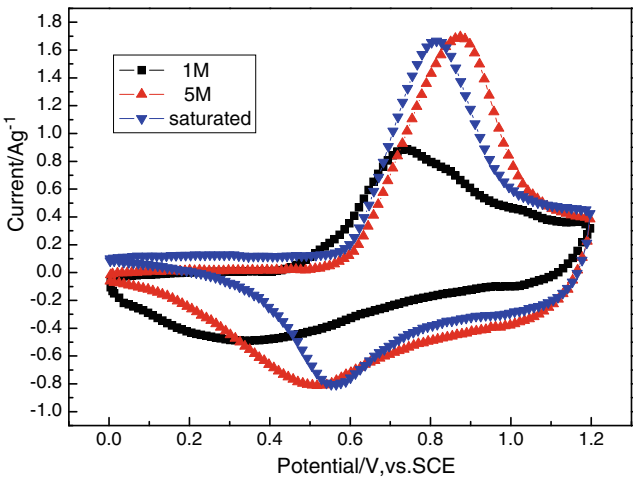

Fig. 3 Comparison of the second cyclic voltammograms of $LiNi_{1/3}Co_{1/3}Mn_{1/3}O_2$ electrode in $LiNO_3$ solutions at different concentrations at a scan rate of 1 mV s^{-1}

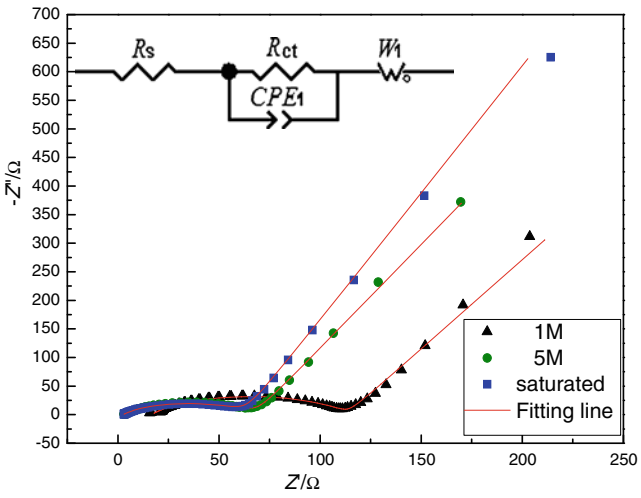

Fig. 4 Nyquist plots of $LiV_{2.9}Ni_{0.050}Mn_{0.050}O_8$//$LiNi_{1/3}Co_{1/3}Mn_{1/3}O_2$ ARLB with $LiNO_3$ solutions at different concentrations and the equivalent circuit model (*inset*)

Table 1 Impedance parameters of $LiV_{2.9}Ni_{0.050}Mn_{0.050}O_8$//$LiNi_{1/3}Co_{1/3}Mn_{1/3}O_2$ ARLB with $LiNO_3$ solutions at different concentrations

Consistency	1 M	5 M	Saturated
R_s/Ω	16.64	2.783	2.586
R_{ct}/Ω	95.64	63.23	59.78

(ox. 1) vs. SCE was observed (see Fig. 5), which are due to the intercalation and deintercalation reaction accompanying gain and loss of electron as shown in the following Eqs. 1 and 2:

$$Li^+\text{intercalation}: LiV_{2.9}Ni_{0.050}Mn_{0.050}O_8 + xLi^+ + xe^- \rightarrow Li_{1+x}V_{2.9}Ni_{0.050}Mn_{0.050}O_8\ (x < 1, \text{at about} - 0.346\,\text{V}) \quad (1)$$

$$Li^+\text{deintercalation}: Li_{1+x}V_{2.9}Ni_{0.050}Mn_{0.050}O_8 \rightarrow LiV_{2.9}Ni_{0.050}Mn_{0.050}O_8 + xLi^+ + xe^-\ (x < 1, \text{at about} - 0.142\,\text{V}) \quad (2)$$

The average redox potential is −0.244 V (vs. SCE). Since hydrogen evolution was observed at the more negative potential, it is clear that $LiV_{2.9}Ni_{0.050}Mn_{0.050}O_8$ is very stable in this aqueous electrolyte and can be used as the negative electrode material without evident hydrogen evolution.

$LiNi_{1/3}Co_{1/3}Mn_{1/3}O_2$ also exhibits one pair of Li^+ intercalation and deintercalation peaks at 0.565 (red. 2) and 0.815 V (ox. 2) vs. SCE (see Fig. 5), respectively (average redox potential of 0.690 V vs. SCE). The reactions are shown in Eqs. 3 and 4:

$$Li^+\text{deintercalation}: LiNi_{1/3}Co_{1/3}Mn_{1/3}O_2 \rightarrow Li_{1-x}Ni_{1/3}Co_{1/3}Mn_{1/3}O_2 + xLi^+ + xe^-\ (x < 1, \text{at about } 0.815\,\text{V}) \quad (3)$$

$$Li^+\text{intercalation}: Li_{1-x}Ni_{1/3}Co_{1/3}Mn_{1/3}O_2 + xLi^+ + xe^- \rightarrow LiNi_{1/3}Co_{1/3}Mn_{1/3}O_2\ (x < 1, \text{at about } 0.565\,\text{V}) \quad (4)$$

These voltages are lower than that for oxygen evolution, which is at approximately 1.8 V versus SCE. This illustrates that the positive electrode is also stable in this aqueous solution.

According to the above discussed, an ARLB can be prepared by using the above two intercalation compounds, i.e., $LiV_{2.9}Ni_{0.050}Mn_{0.050}O_8$ and $LiNi_{1/3}Co_{1/3}Mn_{1/3}O_2$, as the negative and positive electrodes, respectively. Cheap aqueous electrolyte like saturated $LiNO_3$ solution can be used to replace the expensive organic electrolyte. In addition, the safety problems caused by organic electrolyte can be avoided. Cyclic voltammograms of $LiV_{2.9}Ni_{0.050}Mn_{0.050}O_8$//$LiNi_{1/3}Co_{1/3}Mn_{1/3}O_2$ cell with saturated $LiNO_3$ electrolyte at different scan rates are shown in Fig. 6. It can be seen clearly that all the voltammograms of cell in saturated $LiNO_3$ aqueous electrolyte show one pair of obvious redox peaks at different scanning rates (1, 2, 5, and 10 mV s^{-1}), particularly, it can be clearly seen that there is one pair of redox peaks located at 1.2 and 0.7 V even at a high rate of 10 mV s^{-1}. The electrode polarization increases significantly, and the intensity of cathodic and

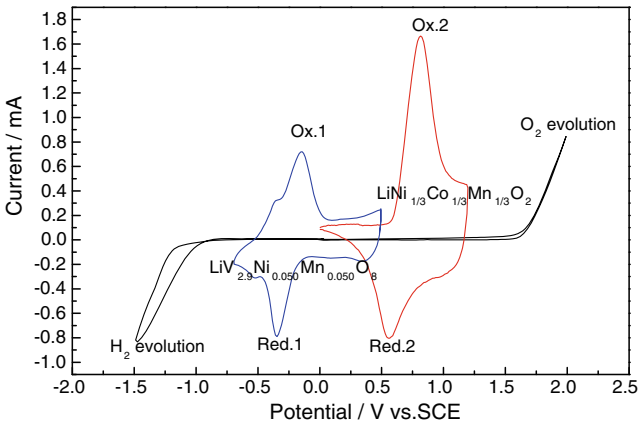

Fig. 5 Cyclic voltammograms of $LiNi_{1/3}Co_{1/3}Mn_{1/3}O_2$ and $LiV_{2.9}Ni_{0.050}Mn_{0.050}O_8$ in the saturated $LiNO_3$ solution electrolyte with a scan rate of 1 mV s^{-1}. Saturated calomel electrode (SCE) was used as the reference electrode and a steel mesh as the counter electrode

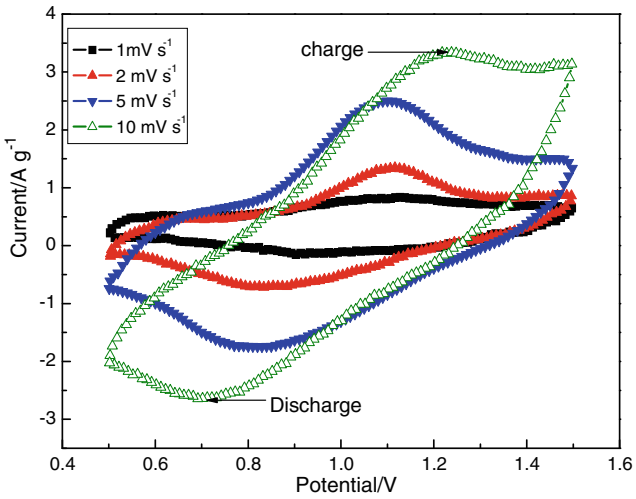

Fig. 6 Cyclic voltammograms of $LiV_{2.9}Ni_{0.050}Mn_{0.050}O_8$//$LiNi_{1/3}Co_{1/3}Mn_{1/3}O_2$ ARLB with saturated $LiNO_3$ electrolyte at different scan rates

anodic peak currents increases gradually as the scan rate increases. The anodic peak shifts from 1.1 to 1.25 V and cathodic peak shifts from 0.9 to 0.7 V with the increase of scan rate. These potentials are less positive than the oxygen evolution potential at about 1.8 V (vs. SCE), and potentials are higher than the hydrogen evolution potential at about −1.2. This indicates that the cell can charge and discharge stably without H_2 or O_2 evolution. The anodic and cathodic peaks corresponding to the following charge and discharge processes, respectively:

$$\text{Charge}: LiNi_{1/3}Co_{1/3}Mn_{1/3}O_2 + LiV_{2.9}Ni_{0.050}Mn_{0.050}O_8 \rightarrow Li_{1-x}Ni_{1/3}Co_{1/3}Mn_{1/3}O_2 + Li_{1+x}V_{2.9}Ni_{0.050}Mn_{0.050}O_8 \quad (x < 1) \tag{5}$$

$$\text{Discharge}: Li_{1-x}Ni_{1/3}Co_{1/3}Mn_{1/3}O_2 + Li_{1+x}V_{2.9}Ni_{0.050}Mn_{0.050}O_8 \rightarrow LiNi_{1/3}Co_{1/3}Mn_{1/3}O_2 + LiV_{2.9}Ni_{0.050}Mn_{0.050}O_8 \quad (x < 1) \tag{6}$$

The charge–discharge curves of $LiV_{2.9}Ni_{0.050}Mn_{0.050}O_8$//$LiNi_{1/3}Co_{1/3}Mn_{1/3}O_2$ cell in different aqueous electrolytes for the first 2 cycles at a rate of 0.5 C (278 mA g^{-1} was assumed to be 1 C rate) are shown in Fig. 7. Though the charge and discharge plateaus are not obvious in Fig. 7, the approximate positions are consistent with the redox peak positions shown in Fig. 7. It can be clearly found that the charge capacity of the first cycle is 176 mAh g^{-1}, which was significant than the discharge capacity (98 mAh g^{-1}), and the coulombic efficiency at the first cycle is calculated to be 55.7%. This behavior indicates the existence of irreversible intercalation sites and irreversible phase transformation at the first cycle, which lead to the low coulombic efficiency. Although the charge capacity of the second cycle is significantly smaller than the first cycle, the discharge capacities are almost the same. The coulombic efficiency of cell at the second cycle increases to 88.1%. And then, the coulombic efficiency of cell is stable at about 92% after 10 cycles (not shown in this study).

Figure 8 shows the cycling stability of $LiV_{2.9}Ni_{0.050}Mn_{0.050}O_8$//$LiNi_{1/3}Co_{1/3}Mn_{1/3}O_2$ ARLB with saturated $LiNO_3$ electrolyte at the rates of 0.2, 0.5, 1.0, 2.0, 3.0, and 5.0 C. The discharge capacity of $LiNi_{1/3}Co_{1/3}Mn_{1/3}O_2$ drops sharply with the increase of charge–discharge rate, which is due to the utilization of active materials, which decrease with the increase of charge–discharge current. The initial discharge capacity of $LiNi_{1/3}Co_{1/3}Mn_{1/3}O_2$ at 0.2, 0.5, 1.0, 2.0, 3.0, and 5.0 C is 103.9, 98.2, 89.1, 74.1, 62.8, and 35.5 mAh g^{-1}, respectively. After 50 cycles, the LiV_3O_8 material delivered the capacities of about 67.5, 63.9, 56.0, 46.3, 43.3, and 19.3 mAh g^{-1} at 0.2, 0.5, 1.0, 2.0, 3.0, and 5.0 C, respectively, corresponding to 64.98%, 65.127%, 62.83%, 62.49%, 68.76%, and 54.34% of the initial capacities.

Although $LiV_{2.9}Ni_{0.050}Mn_{0.050}O_8$//$LiNi_{1/3}Co_{1/3}Mn_{1/3}O_2$ ARLB shows relative good electrochemical properties in saturated $LiNO_3$ solution, further studies are needed to improve its electrochemical performances, such as capacity, coulombic efficiency, and rate capability, especially for cyclability. It has been suggested that the capacity fading is related to transition metal ion dissolution, phase transformation of electrode material, decomposition of water, and etc. [14]. Indeed, a slight dissolution of LiV_3O_8 could be noticed upon finishing galvanostatic investigations, by the change in color, from colorless to slight yellow, of both electrolyte and separator. Nonetheless, the mechanism of

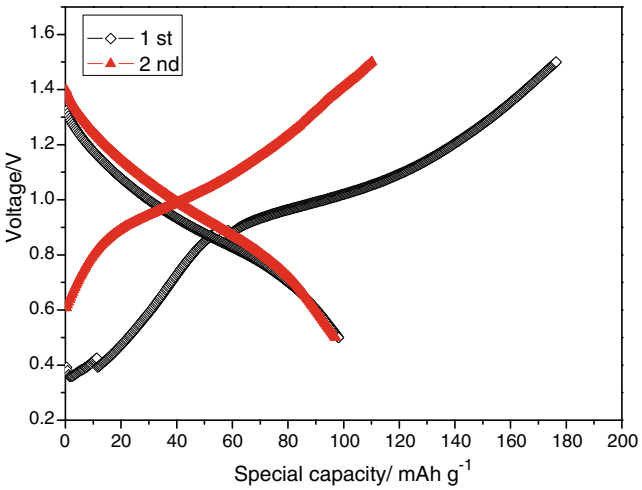

Fig. 7 Charge–discharge curves of $LiV_{2.9}Ni_{0.050}Mn_{0.050}O_8$//$LiNi_{1/3}Co_{1/3}Mn_{1/3}O_2$ ARLB with saturated $LiNO_3$ electrolyte at 0.5 C in the first two cycles

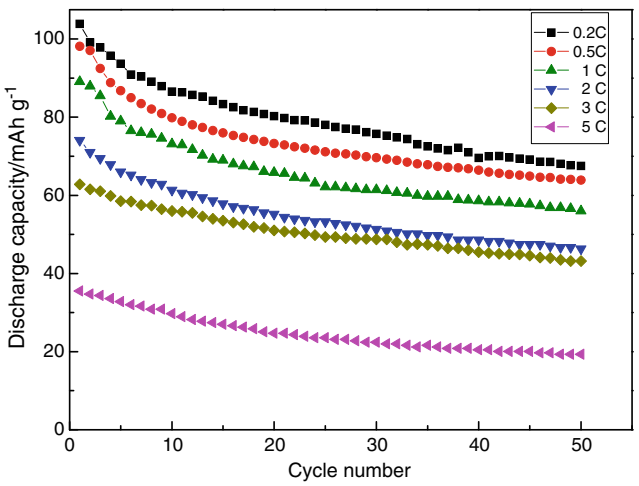

Fig. 8 Cycling behavior of $LiV_{2.9}Ni_{0.050}Mn_{0.050}O_8$//$LiNi_{1/3}Co_{1/3}Mn_{1/3}O_2$ ARLB with saturated $LiNO_3$ electrolyte at various current rates (0.2, 0.5, 1.0, 2.0, 3.0, 5.0 C)

capacity fading on cycling is very complicated, and much more work should be done.

Conclusions

Spherical $LiNi_{1/3}Co_{1/3}Mn_{1/3}O_2$ has been synthesized by a classic co-precipitation method. A pure α-$NaFeO_2$ structure (space group, 166, $R-\overline{3}m$) is observed for as-prepared $LiNi_{1/3}Co_{1/3}Mn_{1/3}O_2$. Electrochemical results indicate that the $LiNi_{1/3}Co_{1/3}Mn_{1/3}O_2$ electrodes in different electrolytes show different electrochemical properties. The electrode in saturated $LiNO_3$ solution exhibits the best electrochemical performance. $LiV_{2.9}Ni_{0.050}Mn_{0.050}O_8$//$LiNi_{1/3}Co_{1/3}Mn_{1/3}O_2$ ARLB with saturated $LiNO_3$ electrolyte is proposed in this work. The cell delivers an initial capacity of 98.2 mAh g^{-1} and retains a capacity of 63.9 mAh g^{-1} after 50 cycles at 0.5 C. Of course, further research is needed to improve the electrochemical properties of this ARLB.

Acknowledgments This work was financially supported by National Natural Science Foundation of China (grant no. 20871101), China Postdoctoral Science Foundation (grant no. 20100480954), Start-up funds for doctor supported by Xiangtan University (grant no. 09QDZ25), Scientific Research Fund of Hunan Provincial Education Department (grant no. 10C1250), Scientific Research Fund of Hunan Province (grant no. 2010RS4027), and Scientific Research Fund of Xiangtan University (grant no. 09XZX10).

References

1. Liu XH, Saito T, Doi T, Okada S, Yamaki J (2009) J Power Sources 189:706–710
2. Zhang S, Li Y, Wu C, Zheng F, Xie Y (2009) J Phys Chem C 113:15058–15067
3. Li W, Dahn JR, Wainwright D (1994) Science 264:1115–1118
4. James G (1994) Science 264:1084
5. Luo JY, Xia YY (2007) Adv Funct Mater 17:3877–3884
6. Kohler J, Makihara H, Uegaito H, Inoue H, Toki M (2000) Electrochim Acta 46:59–65
7. Wang G, Fu L, Zhao N, Yang L, Wu Y, Wu H (2007) Angew Chem Int Ed 46:295–297
8. Ruffo R, Wessells C, Huggins RA, Cui Y (2009) Electrochem Commun 11:247–249
9. Wang GJ, Zhang HP, Fu LJ, Wang B, Wu YP (2007) Electrochem Commun 9:1873–1876
10. Wang Y, Luo J, Wang C, Xia Y (2006) J Electrochem Soc 153: A1425–A1431
11. Wang GJ, Fu LJ, Wang B, Zhao NH, Wu YP, Holze R (2008) J Appl Electrochem 38:579–581
12. Nakayama N, Yamada I, Huang Y, Nozawa T, Iriyam Y, Abe T, Ogumi Z (2009) Electrochim Acta 54:3428–3432
13. Wang H, Huang K, Zeng Y, Yang S, Chen L (2007) Electrochim Acta 52:3280–3285
14. Wang H, Zeng Y, Huang K, Liu S, Chen L (2007) Electrochim Acta 52:5102–5107
15. Wang GJ, Qu QT, Wang B, Shi Y, Tian S, Wu YP, Holze R (2009) J Power Sources 189:503–506
16. Wang GJ, Zhao NH, Yang LC, Wu YP, Wu HQ, Holze R (2007) Electrochim Acta 52:4911–4915
17. Tang W, Liu LL, Tian S, Li L, Yue YB, Wu YP, Guan SY, Zhu K (2010) Electrochem Commun 12:1524–1526
18. Luo JY, Cui WJ, He P, Xia YY (2010) Nat Chem 2:760–765
19. Minakshi M, Singh P, Mitchell DRG, Issa TB, Prince K (2007) Electrochim Acta 52:7007–7013
20. Wang GJ, Qu QT, Wang B, Shi Y, Tian S, Wu YP, Holze R (2009) Electrochim Acta 54:1199–1203
21. Tian L, Yuan A (2009) J Power Sources 192:693–697
22. Lee M-H, Kang Y-J, Myung S-T, Sun Y-K (2004) Electrochim Acta 50:939–948
23. Henriksen G, Amine K, Liu J, Nelson P (2003) Abstract 255. Presented at the 204th Meeting of the Electrochemical Society, Orlando, 12–16 October 2003
24. Luo X, Wang X, Liao L, Wang X, Gamboa S, Sebastian PJ (2006) J Power Sources 161:601–605
25. Liao L, Wang X, Luo X, Wang X, Gamboa S, Sebastian PJ (2006) J Power Sources 160:657–661
26. Park S-H, Shin H-S, Myung S-T, Yoon CS, Amine K, Sun Y-K (2005) Chem Mater 17:6–8
27. Park SH, Kang SH, Belharouak I, Sun YK, Amine K (2008) J Power Sources 177:177–183
28. Zheng J, Chen J, Jia X, Song J, Wang C, Zheng M, Dong Q (2010) J Electrochem Soc 157:A702–A706
29. Liu L, Jiao L, Sun J, Zhao M, Zhang Y, Yuan H, Wang Y (2008) Solid State Ionics 178:1756–1761
30. Ohzuku T, Ueda A, Nagayama M (1993) J Electrochem Soc 140:1862–1870
31. Cho TH, Park SM, Yoshio M, HiraiI T, Hideshima Y (2005) J Power Sources 142:306–312
32. Wu MS, Lee RH (2008) J Power Sources 176:363–368
33. Chen CH, Liu J, Amine K (2001) J Power Sources 96:321–325